ChemPubSoc Europe

DOI: 10.1002/open.201900141

Open Access ChemistryOPEN Communications

Acceptor Derivatization of the 4CzIPN TADF System: Color Tuning and Introduction of Functional Groups

Fabian Hundemer[+],[a] Lorenz Graf von Reventlow[+],[b, c] Céline Leonhardt,[a] Mika Polamo,[d] Martin Nieger,[d] Stefan M. Seifermann,*[a] Alexander Colsmann,*[b, c] and Stefan Bräse*[a, c, e]

We demonstrate modular modifications of the widely employed emitter 2,4,5,6-tetra(9*H*-carbazol-9-yl)isophthalonitrile (4CzIPN) by replacing one or both nitrile acceptors with oxadiazole groups via a tetrazole intermediate. This allows the introduction of various functional groups including halides, alkynes, alkenes, nitriles, esters, ethers and a protected amino acid while preserving the thermally activated delayed fluorescence (TADF) properties. The substituents control the emission maximum of the corresponding emitters, ranging between 472–527 nm, and show high solid-state photoluminescence quantum yields up to 85%. The TADF emission of two compounds, 4CzCNOXDtBu and 4CzdOXDtBu, a mono- and a bis-oxadiazole substituted 4CzIPN is characterized in detail by time- and temperature-dependent photoluminescence. Solution-processed OLEDs comprising 4CzCNOXDtBu and 4CzdOXDtBu show a significant blue-shift of the emission compared to the reference 4CzIPN, with external quantum efficiencies of 16%, 5.9% and 17% at 100 cd m^{-2}, respectively.

1. Introduction

Luminescent molecules featuring thermally activated delayed fluorescence (TADF) are promising candidates to achieve efficient and economically viable organic light-emitting diodes (OLEDs) omitting expensive rare-earth metals.[1–4] To enable an efficient use of triplet states, TADF emitters feature an efficient reverse intersystem crossing (RISC) from the triplet to the singlet state at room temperature. This is enabled by incorporation of donor and acceptor groups in a highly twisted configuration within a single molecule, thus reducing the coupling of the highest occupied molecular orbital (HOMO) and lowest unoccupied molecular orbital (LUMO) and hence, the gap between the singlet and the triplet state (ΔE_{ST}). Earlier reports pointed out that the emission properties of TADF molecules can be tuned by donor modifications. For example, the substitution of the carbazole units with alkyl and aryl moieties on the well-investigated and highly efficient 2,4,5,6-tetra(9*H*-carbazol-9-yl)isophthalonitrile (4CzIPN) leads to a shift of the emission wavelength,[1] while the incorporation of halides lead to a significant shortening of the excited state lifetimes.[5]

In 4CzIPN, nitrile units serve as efficient acceptor moieties. From a synthetic point of view, nitriles are also valuable access points to further modify the conjugated TADF system, to tune the solubility or to attach a cross-linking moiety. Recently, Zysman-Colman *et al.* reported a two-step protocol, to replace the nitriles by oxadiazoles in 1,2-bis(carbazol-9-yl)-4,5-dicyanobenzene (2CzPN) for deep-blue emitters. These emitters exhibited emission maxima at 474 nm and 446 nm and maximum external quantum efficiencies (EQE) of 11.2% and 6.6%, respectively.[6] Most recently, the Zysman-Colman group expanded this concept to derivatives of another isomer of 2CzPN.[7]

The group of Kippelen reported the combination of *tert*-butylphenyl-substituted oxadiazole acceptors and carbazole donors. The resulting TADF emitter exhibited an emission maximum in toluene at 569 nm and a photoluminescence quantum yield (PLQY) of 71% in neat thin-films. The corresponding OLEDs with a host-free emission layer produced a maximum EQE of 21%. This was further improved upon embedding of the emitter into a host at 40 wt% to 28% EQE.[8] Replacing the nitrile groups by the less electron-withdrawing oxadiazole units with weaker acceptor strength[9,10] results in a bluer emission and promising thermal and electron transport properties[9,11–16] as predicted by advanced theoretical calculations.[1,9,13]

In this report, we transfer this substitution concept to 4CzIPN to master two important challenges: Firstly, the nitrile groups in 4CzIPN are sterically more shielded and hence synthetically less accessible compared to 2CzPN. If successful, we expect these transformations to be also applicable to

[a] *F. Hundemer,[+] C. Leonhardt, S. M. Seifermann, Prof. Dr. S. Bräse*
Institute of Organic Chemistry, Karlsruhe Institute of Technology (KIT), Fritz-Haber-Weg 6, 76131 Karlsruhe, Germany
Tel: (+49)-721-608-42903
E-mail: braese@kit.edu
[b] *L. Graf von Reventlow,[+] A. Colsmann*
Karlsruhe Institute of Technology (KIT), Light Technology Institute, Engesserstrasse 13, 76131 Karlsruhe, Germany
[c] *L. Graf von Reventlow,[+] A. Colsmann, Prof. Dr. S. Bräse*
Karlsruhe Institute of Technology (KIT), Material Research Center for Energy Systems, Strasse am Forum 7, 76131 Karlsruhe, Germany
[d] *M. Polamo, M. Nieger*
Department of Chemistry, University of Helsinki, P. O. Box 55, 00014 University of Helsinki, Finland
[e] *Prof. Dr. S. Bräse*
Institute of Toxicology and Genetics, Karlsruhe Institute of Technology (KIT), Hermann-von-Helmholtz-Platz 1, D-76344 Eggenstein-Leopoldshafen, Germany
[+] *These authors contributed equally to this work.*

Supporting information for this article is available on the WWW under https://doi.org/10.1002/open.201900141

analogous emitter motifs, featuring the nitrile functions also in a sterically demanding arrangement. Secondly, being one of the most commonly used TADF emitters in OLEDs, 4CzIPN possesses excellent photophysical properties. Introducing the versatile oxadiazole group to 4CzIPN provides a handle to a targeted fine-tuning of its properties. Accordingly, we introduced a variety of oxadiazole modifications and structural motives to show the feasibility of this method with regard to functional group tolerance and to study their influence on the photophysical properties.

2. Results and Discussion

2.1. Synthesis

The reference emitter 4CzIPN was synthesized following previous literature reports.[1] Although there are many synthetic routes for the synthesis of oxadiazole groups,[17–19] a two-step protocol using tetrazole turned out to be most feasible, given the presence of the nitrile groups. 4CzIPN was reacted with sodium azide and copper sulfate as catalyst in DMSO at 140 °C overnight to yield the tetrazole derivative **2** with the mixed acceptor motif featuring a tetrazole.[20] Subsequently, the tetrazole reacted with various acyl chlorides to yield a large scope of the targeted oxadiazole-modified 4CzIPN.[21] (Scheme 1)

Carboxylic acids can also be used to transform the tetrazole to oxadiazole by addition of a carbodiimide reagent like *N,N'*-diisopropylcarbodiimide (DIC).[22] Using this method, a plethora of functional groups and structural motives, which otherwise are expensive or unavailable by the acyl chloride route, can be added to the emitters. In this work, we studied the introduction of an alkyne, using propiolic acid which acyl acid derivative is unavailable as well as the usage of a protected amino acid to show the compatibility with larger biomolecules.

The substituents at the oxadiazole were chosen following three rationales: Firstly, electron withdrawing and donating groups were used to study their influence on the optoelectronic properties. For that we incorporated alkyl chains (4CzCNOXD $(CH_2)_{10}CH_3$, 4CzCNOXDtBu) and electron-donating arenes (4CzCNOXD2,6OMePh, 4CzCNOXDMes). As electron withdrawing moieties, perfluorinated alkyl chains (4CzCNOXD$(CF_2)_6CF_3$) and electron-donating arenes were used (4CzCNOXD4CNPh, 4CzCNOXDC_6F_5). Secondly, in order to demonstrate the feasibility of this method, the steric hinderance and complexity of the acyl chlorides was investigated. Hence, sterically demanding acyl chlorides such as pivaloyl chloride, 2,4,6-trimethylbenzoyl chloride and 2,6-dimethoxybenzoyl chloride were used to yield the respective oxadiazoles in good to high yields. Thirdly,

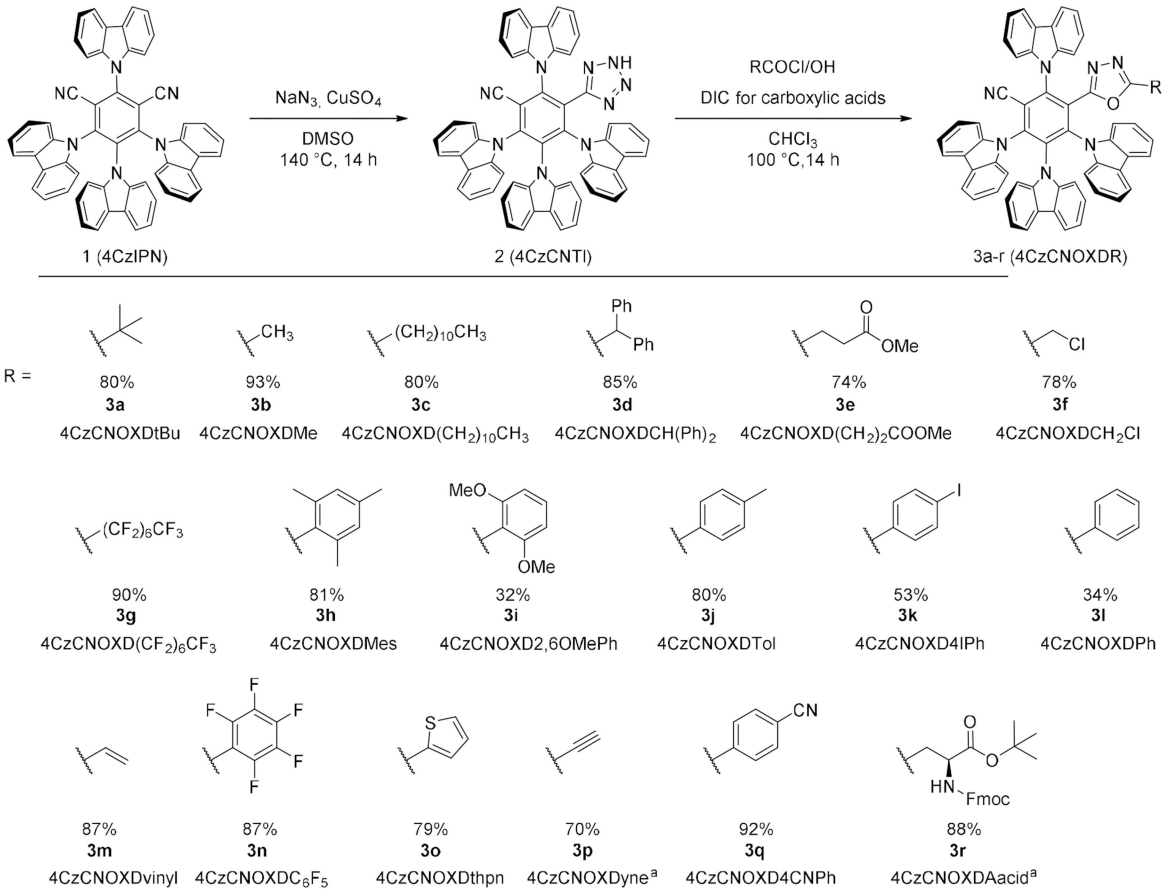

Scheme 1. Synthesis of mono-oxadiazole derivatives of 4CzIPN in a two-step protocol. a: reaction starting from the respective carboxylic acid.

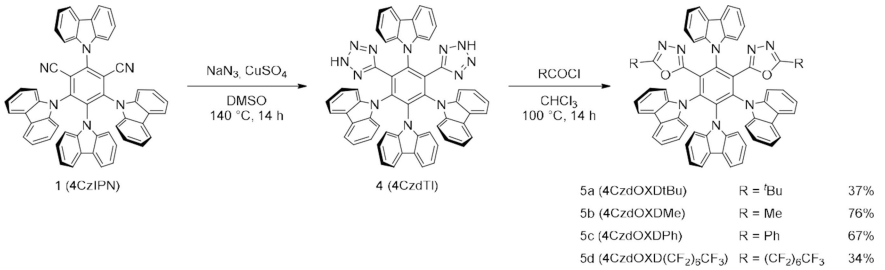

Scheme 2. Synthesis of the bis-oxadiazole derivatives of 4CzIPN following a two-step protocol.

functional groups and structural motives like esters, ethers, nitriles, alkenes, alkynes, halides, heterocycles and a protected amino acid were tolerated and successfully conjoined to the respective oxadiazole.

In four products, both nitrile moieties in 4CzIPN were replaced by oxadiazole groups. By adjusting the equivalents of sodium azide in the first step, 4CzIPN can also easily be transformed into 4CzdTI which was then reacted according to the previous procedure (Scheme 2).

Single crystals, suitable for X-ray analysis were obtained for 4CzCNOXDMe, 4CzCNOXD2,6OMePh, 4CzCNOXDMes, 4CzCNOXDC$_6$F$_5$ and 4CzCNOXDCH$_2$Cl. All reported compounds show similar arrangements, with the carbazole rings being strongly twisted in regard to the central benzene ring (Figure 1).

The dihedral angles of all carbazoles were similar throughout the series of different oxadiazole derivatives, usually ranging from 64.4–70.1°. The oxadiazole heterocycles in all five emitters were less twisted compared to the carbazoles due to their smaller size, resulting in less steric repulsion with the neighboring groups and the central benzene core, showing dihedral angles between 41.9° and 54.4°. In 4CzCNOXD2,6OMePh and 4CzCNOXDMes, the arene substituents on the oxadiazoles were twisted with dihedral angles of 62.3° and 59.8°, respectively, due to the steric repulsion of the methoxy and methyl groups in ortho position to the link to the oxadiazole. In 4CzCNOXDC$_6$F$_5$, the pentafluoro benzene was oriented almost coplanar at an angle of 14.7° due to little steric repulsion, also indicating a certain degree of conjugation between these ring systems.

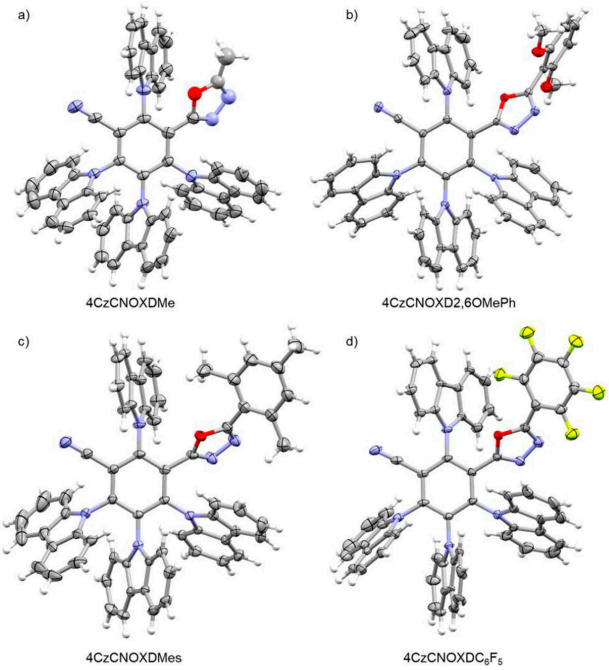

Figure 1. Molecular structure of a) 4CzCNOXDMe, b) 4CzCNOXD2,6OMePh, c) 4CzCNOXDMes and d) 4CzCNOXDC$_6$F$_5$ – (minor disordered parts were omitted for clarity, displacement parameters are drawn at 50% probability level).

2.2. Theoretical Calculations

For a first assessment of their usability in OLEDs and other light-emitting applications, we have predicted the optoelectronic properties of selected emitters by DFT calculations (Figure 2). Similar to 4CzIPN, the HOMO is located on the carbazole-donors. Some molecular orbitals are formed partially delocalized over several carbazole moieties (HOMO, HOMO-1, HOMO-2, etc.). As reported by the Zysman-Colman group, oxadiazoles are known to be weaker acceptor groups than nitriles.[6] The oxadiazoles are expected to destabilize the LUMO, increasing its energy and the optical band gap. For the mono-oxadiazole substituted derivative of 4CzIPN, the LUMO is partially located on the oxadiazole moiety and mainly located on the benzonitrile, whereas, for the bis-oxadiazole derivative, the LUMO is mostly located on the oxadiazole heterocycles and the respective benzene core. While the HOMO energies slightly increase from −5.82 eV in 4CzIPN to −5.75 eV for 4CzCNOXDtBu and to −5.66 eV for 4CzdOXDtBu, we found a significant destabilization of the LUMO orbital upon replacing one or both nitrile groups by oxadiazoles of 0.22 eV and 0.51 eV, respectively, resulting in an increased optical band gap of 3.26 eV for 4CzCNOXDtBu and 3.46 eV for 4CzdOXDtBu compared to 3.11 eV for the reference emitter 4CzIPN. Experimentally measured HOMO energies, determined by photoelectron spectroscopy in air (PESA) on thin-films are in very close agreement (−5.82 eV for 4CzCNOXDtBu and −5.75 eV for 4CzdOXDtBu). Both calculated ΔE_{ST} are reasonably low with 0.08 eV and 0.13 eV for RISC to occur and similar to 4CzIPN (0.12 eV), which makes them promising candidates for triplet harvesting in OLEDs.

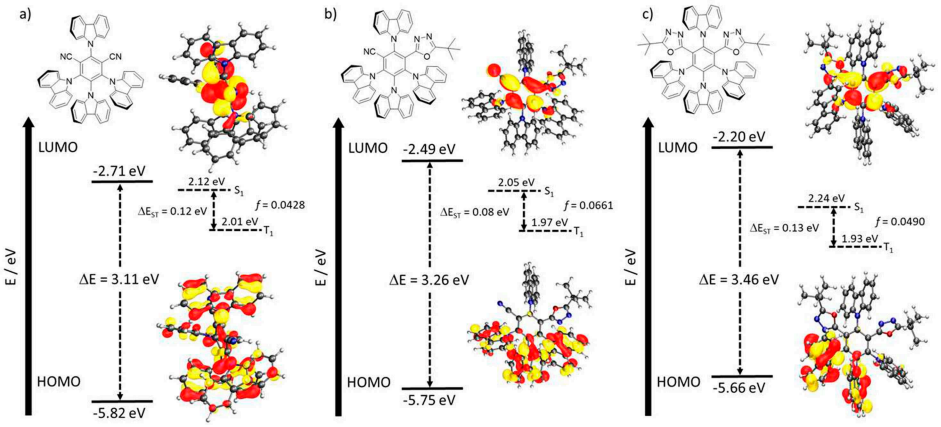

Figure 2. DFT calculations of a) 4CzIPN, b) the mono-oxadiazole derivative 4CzCNOXDtBu and c) the bis-oxadiazole derivative 4CzdOXDtBu.

2.3. Photophysical Properties

To investigate the photophysical properties of the various emitters with different structural modifications, the oxadiazole emitters were studied in solid state (Supporting Information Table 1). Therefore, thin-films were prepared by spin-coating a 10 wt% poly(methyl methacrylate) (PMMA) solution doped with emitter molecules.

All mono-oxadiazole derivatives of 4CzIPN show a high PLQY of 66–85%, except for 4CzCNOXDvinyl (21%). The emission maxima varied between 498 nm for 4CzCNOXDtBu and 527 nm for 4CzCNOXD$(CF_2)_6CF_3$ depending on the electron donating or withdrawing character of the group attached to the oxadiazole. The emission maximum of 4CzIPN was found at 516 nm with a PLQY of 89%. As depicted in Figure 3, independent of their hybridization state, the attached electron donating groups (alkyl, mesityl, methoxy, toluyl, phenyl) led to a blue-shift of the emission versus derivatives having electron withdrawing groups such as halides, perfluorinated alkyl or aryl groups, and nitriles.

The bis-oxadiazole derivatives of 4CzIPN exhibited an even stronger blue-shift than the mono-oxadiazole derivatives, as shown in Figure 3 for 4CzdOXDtBu, 4CzdOXDMe, 4CzdOXDPh and 4CzdOXD$(CF_2)_6CF_3$ (472 nm vs. 498 nm, 482 nm vs. 499 nm, 490 nm vs. 506 nm and 523 nm vs. 527 nm) and as predicted by

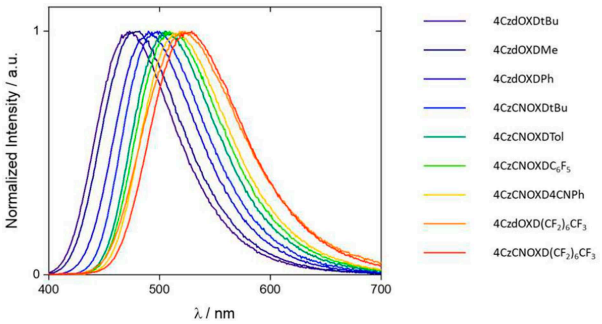

Figure 3. Emission spectra of selected mono- and bis-oxadiazole derivatives of 4CzIPN.

DFT-calculations. The bis-oxadiazole derivatives exhibited a slightly lower PLQY with 48–74% than the mono-oxadiazole derivatives.

The TADF properties of two molecules of the series were studied in detail, a mono- and a bis-oxadiazole derivative containing the same acceptor-modification group (4CzCNOXDtBu (**3a**) and 4CzdOXDtBu (**5a**)). We chose these two emitters because the blue shift of the emission spectrum was strongest, both showed rather short delayed fluorescence lifetimes and high PLQYs. We also wanted to investigate in more detail the influence of a second oxadiazole modification (bis-oxadiazole derivative) on the emission properties. Time- and temperature dependent photoluminescence was measured on solution processed thin-films (10 wt% emitter in 1,3-bis(*N*-carbazolyl) benzene (mCP)) on quartz substrates. Upon embedding of the emitter molecules in mCP, the PLQY of both (57% for 4CzCNOXDtBu and 29% for 4CzdOXDtBu) was reduced versus the incorporation into a matrix of PMMA (85% and 50%). The PLQY of charge-transfer-state emitters strongly depends on the molecular environment, such as its polarity, which makes the choice of a suitable host very important.[23–25] E.g. when embedded into 3,3′-di(9*H*-carbazol-9-yl)-1,1′-biphenyl (m-CBP) instead, the PLQY is reduced drastically (34% and 15%). In mCP, both molecules show a fast and a slow emission component (Figure 4a). Both exhibit a rather short delayed fluorescence lifetime of 2.8 µs which is very important for OLED applications. Molecules with excited-state lifetimes in the long micro- or even millisecond range are unsuitable for OLEDs as they induce a strong efficiency roll-off originating from bimolecular quenching mechanisms like triplet-triplet or triplet-polaron annihilation.[26] The activation energy of the RISC provides an estimation of ΔE_{ST} and can be obtained from an Arrhenius fit as depicted in Figure 4b. The RISC rate k_{RISC} is calculated by the formula in the inset of Figure 4b, where I_{DF} and I_{PF} are the integrated intensities of the delayed and prompt emission components. τ_{DF} is the lifetime of the delayed fluorescence. For compounds **3a** and **5a** ΔE_{ST} yields 52 ± 10 meV and 59 ± 10 meV, respectively, which slightly differ from the values obtained by DFT calculations in the gas phase

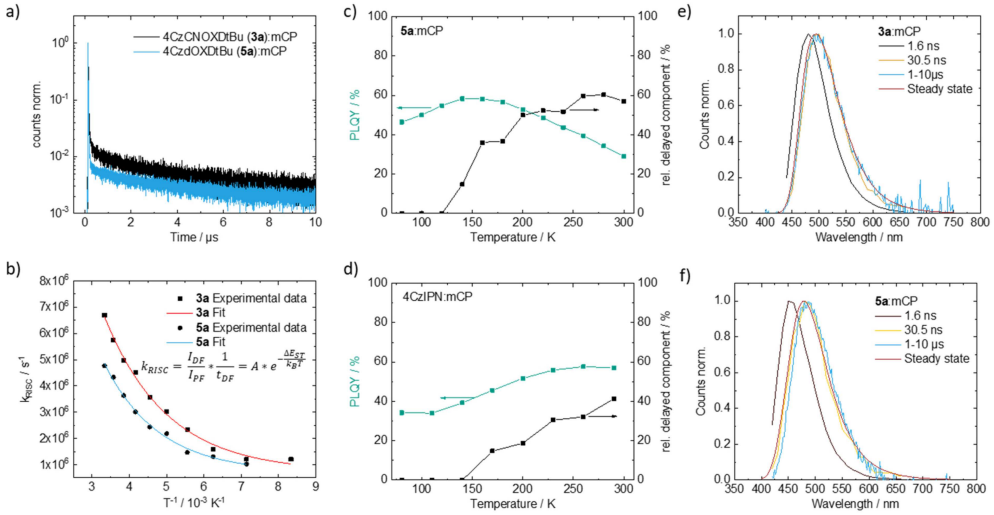

Figure 4. a) Photoluminescence decay of compounds **3a** and **5a** in mCP at room temperature. The samples were excited at 340 nm and the PL-decays were measured at 500 nm (**3a**) and 480 nm (**5a**). b) Arrhenius plot of the RISC rate over the inverse temperature and calculation of the TADF activation energy. c,d) Temperature dependent PLQY and delayed fluorescence component of **5a** and 4CzIPN in mCP. e,f) Emission spectra of compound **3a** and **5a** after 1.6 ns, 30.5 ns and 1–10 µs as well as the steady-state emission spectrum.

(ΔE_{ST} = 80 meV and 130 meV). The experimentally determined singlet-triplet gaps are close to the reference molecule 4CzIPN (ΔE_{ST} = 83 meV), demonstrating that important TADF properties prevail upon introduction of oxadiazole moieties to 4CzIPN.[1] We note that the uncertainty of the experimentally determined data reflects uncertainties of the fits but not of the measurement setup. We observed no delayed emission from both components below 120 K, indicating that TADF is the dominant mechanism of the delayed emission at common operation temperature. Intensity-dependent photoluminescence at room temperature produced a slope close to one in a double logarithmic plot, indicating monomolecular recombination, hence ruling out triplet-triplet annihilation as the origin for the delayed emission (Figure S1).

To investigate why compound **5a** exhibits a much lower PLQY than compound **3a** or 4CzIPN, we measured the PLQY temperature dependent. As depicted in Figure 4c, **5a** in mCP exhibits a PLQY maximum of 58% at 140 K where only a small portion of delayed fluorescence is visible even though a substantial amount of singlet excitons is lost to intersystem crossing to the triplet state which decays mostly non-radiative (Figure 4c). This is a clear indication that the low PLQY mostly stems from a non-radiative (vibronic) decay of the singlet state and not from an inefficient RISC. In the case of 4CzIPN, the PLQY drops with temperature at the same rate as the delayed fluorescence (Figure 4d). Seemingly, the second oxadiazole group induces more vibrations in the molecule which leads to an enhanced deactivation of the singlet state, whereas it barely affects k_{RISC}.

Interestingly, both **3a** and **5a** in mCP showed two fast decay components which can be attributed to prompt fluorescence in the short ns-regime. This behavior is not visible if the compounds are dissolved in tetrahydrofuran (Figure S2). To investigate the origin of the two decay times, time-resolved emission spectra (TRES) were recorded using time-resolved single-photon counting (TCSPC). TCSPC measurements were carried out at different emission wavelengths with constant measurement time to resolve the spectra in different time regimes after excitation. Clearly, in Figure 4e, a red-shift in the spectrum from 480 nm to 498 nm of compound **3a** is visible within the first few nanoseconds. After 30 ns the spectral shape of the emission remains constant and the delayed component (1–10 µs) also matches the spectrum of the second prompt component. The complete TRES data up to 200 ns is shown in Figure S2 in the Supporting Information. The steady-state emission nearly matches the second prompt and the delayed component because the intensity of the first component is rather low. A similar behavior was also seen in other TADF molecules with a donor-acceptor-donor structure[27] and in exciplex-TADF systems.[28] Hence, we propose the emission mechanisms of **3a** to work as follows: Upon excitation of the sample, mostly singlet excitons on mCP are generated because the emitter concentration is low (10 wt%). This energy is transferred via Förster transfer to compound **3a**. The energy transfer to a local excited singlet state (^{1}LE) on **3a** appears to be more efficient than a transfer directly to the charge-transfer singlet state (^{1}CT). Energy transfer from the ^{1}LE to the energetically more favorable ^{1}CT state follows subsequently. Due to the twisted arrangement of the individual TADF molecules and hence due to the weak coupling of the involved states, this process is extremely slow, which is why the energy transfer competes with fluorescence from the ^{1}LE state which is visible in Figure 4e (t < 30 ns).[27] After this time the emission spectrum remains constant. Since the molecules have a higher degree of freedom in solution than in the solid state, the coupling of ^{1}LE and ^{1}CT may be enhanced, extinguishing the emission from ^{1}LE in solution (Figure S2). All spectra between 1.6 ns and 30 ns in mCP can be modelled by a linear combination of the spectra at

1.6 ns and 30 ns (Figure S2), which is another indication that the fluorescence arises from two separate states. To rule out that the fast fluorescence arises from a CT state between host and guest we also measured TRES of **3a**:m-CBP. Here, all spectra match nearly perfectly with **3a**:mCP (Figure S2).

Compound **5a** behaves similar to **3a** with emission occurring from two different states which we again propose to be a ^{1}LE and the ^{1}CT state (Figure 4f). Whether the fluorescent ^{1}LE state is located on the donor or acceptor units remains to be shown. Notably, 4CzIPN behaves similar when doped into mCP (Figure S3) which is why the oxadiazole substitution of the molecule cannot be the origin of the emission characteristics. Sandanayaka et al. also observed more than one fast PL decay component in the ns-range with emission at wavelengths below 500 nm of 4CzIPN in m-CBP but did not investigate it further.[29]

2.4. Electroluminescence in OLEDs

As the newly designed TADF molecules showed very high solubility (>3 g/L in THF), we chose deposition from solution for the fabrication of OLEDs. Their high solubility provides a great advantage over phosphorescent iridium complexes which are commonly used in OLEDs and which have very often only limited solubility (<1 g/L), thus avoiding strong molecular aggregation and hence quenching of excited triplet states.[30] In light of its good photophysical properties, we chose the host mCP as discussed above.[4] We implemented the emission layer into a regular architecture (bottom ITO anode) comprising a hole-transport layer from spin-cast poly(3,4-ethylenedioxythiophene):polystyrene sulfonate (PEDOT:PSS), a vacuum-deposited electron transport layer from 3,3′,5,5′-tetra[(m-pyridyl)-phen-3-yl]biphenyl (BP4mPy) and a 8-hydroxyquinolinolato-lithium (Liq)/Aluminum cathode. After optimization of the emission layer and electron transport layer thicknesses, the emitter concentration and the annealing temperatures, the OLEDs comprising **3a** achieved an EQE of 16% at 100 cd m^{-2} and an EQE of 5.9% if **5a** was used instead. For reference, 4CzIPN-based reference OLEDs achieved an EQE of 17% at the same luminance. Figure 5 depicts the optoelectronic properties of the OLEDs. All devices showed only negligible efficiency roll-off in the EQE up to 300 cd m^{-2} which is in the brightness range of OLED displays. We note that the EQE = 16% of **3a** exceeded expectations since the previously measured PLQY yielded 57%. Usually, the PLQY is integrated over the whole thickness of the emissive layer whereas the emission zone in an OLED is often much narrower.[31] And as it is unlikely in solution processed host:guest systems that the emitters are homogenously distributed, the molecular environment in the emission zone can differ from the rest of the layer and the PLQY can locally be higher. We note that, while in general 4CzIPN-OLEDs can be rather stable,[32] here, additional work on the optimization of the layer stack will be needed in the future to also enhance the OLED lifetime (LT50 in the range of minutes at 300 cd m^{-2}, Figure S4). In particular the acidity of the PEDOT:PSS hole transport layer and the concomitant release of ion from the ITO electrode as well as some solvent residues, may have fostered device degradation.

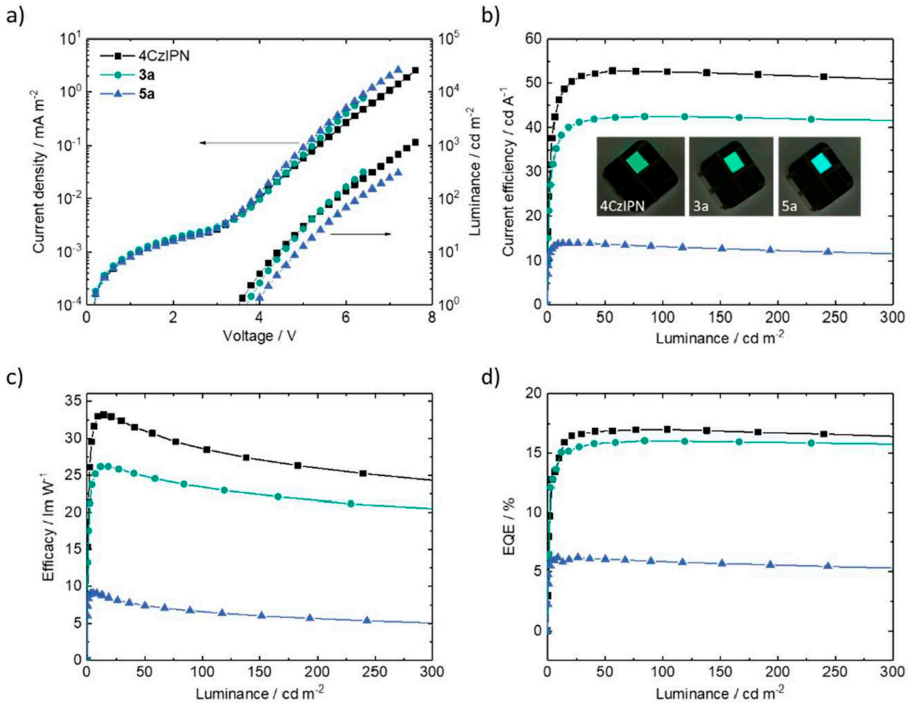

Figure 5. a) J–V (left axis) and L–V characteristics (right axis) of solution processed OLEDs containing either of the emitters 4CzIPN, **3a** and **5a**. b) Current efficiency. Inset: photos of OLEDs containing 4CzIPN, **3a** and **5a** (from left to right). The color shift is clearly visible. c) Efficacy and d) EQE. All graphs represent the second measurement of the devices, and the current densities were kept moderate to prevent degradation of the OLEDs during the measurements.

3. Conclusion

This work shows the feasibility of and the opportunities arising from the replacement of nitriles in the widely used 4CzIPN TADF emitter by oxadiazole acceptors. The additional degrees of freedom in molecular design can be used to promote a significant blue-shift of the emission while maintaining high fluorescence quantum yields. Either one or both nitriles can be selectively replaced by oxadiazoles. The emitters 4CzCNOXDtBu and 4CzdOXDtBu which feature alkylated oxadiazole substituents, show TADF. The corresponding solution processed OLEDs produced maximum EQEs of 16% and 5.9% at 100 cd m^{-2}. Importantly, the devices exhibited only negligible efficiency roll-off up to 300 cd m^{-2} due to a short delayed fluorescence lifetime of 2.8 µs. Low excited state lifetimes are one of the key parameters for the design of new light-emitting molecules for OLED applications. We attribute the lower efficiency of the bluer device comprising 4CzdOXDtBu to the second oxadiazole group which induces vibrational modes that enhance the non-radiative decay from the singlet state, resulting in lower PLQY.

Experimental Section

4CzCNTI

In a vial, 4CzIPN (2.00 g, 2.54 mmol, 1.00 equiv.), sodium azide (330 mg, 5.07 mmol, 2.00 equiv.) and copper sulfate (40.0 mg, 0.254 mmol, 0.10 equiv.) were sealed and flushed with argon three times. Subsequently, dimethyl sulfoxide (15 mL) was added. The mixture was stirred at 140 °C for 14 h. Afterwards, the solution was added to water, carefully acidified with hydrochloric acid and extracted with dichloromethane (2×100 mL). The combined organic layers were washed with brine, dried over sodium sulfate and concentrated under reduced pressure. The crude product was purified by column chromatography on silica gel (ethyl acetate/dichloromethane 0–100%). The crude product was washed with cold ethyl acetate to obtain the product as a yellow solid in 1.53 g (69%) yield.

General Procedure 1

The starting material and acyl chloride were added to trichloromethane and sealed in a vial. The mixture was heated and stirred at 100 °C for 14 h. The reaction mixture was poured into saturated aqueous sodium hydrogen carbonate solution and stirred for 15 minutes. The organic layer was washed with brine, dried over Na_2SO_4 and concentrated under reduced pressure. The crude product was purified by column chromatography on silica gel (cyclohexane/DCM) to obtain the respective oxadiazole.

General Procedure 2

The starting material, carboxylic acid and *N,N'*-Diisopropylcarbodiimide were added to trichloromethane and sealed in a vial. The mixture was heated and stirred at 100 °C until full conversion. The reaction mixture was poured into saturated aqueous sodium hydrogen carbonate solution and stirred for 15 minutes. The organic layer was washed with brine, dried over Na_2SO_4 and concentrated under reduced pressure. The crude product was purified by column chromatography on silica gel (cyclohexane/DCM) to obtain the respective oxadiazole.

Supporting Information Contain General Information, Experimental Procedures and Additional Analytical Data

CCDC 1873988 (4CzCNOXDMe), 1873989 (4CzCNOXD2,6-MeOPh), 1873990 (4CzCNOXDMes), 1873991 (4CzCNOXDC$_6$F$_5$), and 1873992 (4CzCNOXDCH$_2$Cl) contain the supplementary crystallographic data for this paper. These data can be obtained free of charge from The Cambridge Crystallographic Data Centre via www.ccdc.cam.ac.uk/data_request/cif.

Acknowledgements

F. H., A. C. and S. B. acknowledge funding from DFG in the frame of SFB1176 (projects A4, B3, C2 and C6).

Conflict of Interest

The authors declare no conflict of interest.

Keywords: thermally activated delayed fluorescence · organic light emitting diodes (OLED) · oxadiazoles · color-tuning · functionalization

[1] H. Uoyama, K. Goushi, K. Shizu, H. Nomura, C. Adachi, *Nature* **2012**, *492*, 234–238.
[2] X. Cai, S.-J. Su, *Adv. Funct. Mater.* **2018**, *28*, 1802558.
[3] T. Huang, W. Jiang, L. Duan, *J. Mater. Chem. C* **2018**, *6*, 5577–5596.
[4] M. Y. Wong, E. Zysman-Colman, *Adv. Mater.* **2017**, *29*, 1605444.
[5] A. Kretzschmar, C. Patze, S. T. Schwaebel, U. H. F. Bunz, *J. Org. Chem.* **2015**, *80*, 9126–9131.
[6] M. Y. Wong, S. Krotkus, G. Copley, W. Li, C. Murawski, D. Hall, G. J. Hedley, M. Jaricot, D. B. Cordes, A. M. Z. Slawin, *ACS Appl. Mater. Interfaces* **2018**, *10*, 33360–33372.
[7] Z. Li, W. Li, C. Keum, E. Archer, B. Zhao, A. M. Z. Slawin, W. Huang, M. C. Gather, I. D. W. Samuel, E. Zysman-Colman, *J. Phys. Chem. C* **2019**, *123*, 24772–24785.
[8] X. Zhang, M. W. Cooper, Y. Zhang, C. Fuentes-Hernandez, S. Barlow, S. R. Marder, B. Kippelen, *ACS Appl. Mater. Interfaces* **2019**, *11*, 12693–12698.
[9] Y. Zhang, C. Zuniga, S.-J. Kim, D. Cai, S. Barlow, S. Salman, V. Coropceanu, J.-L. Brédas, B. Kippelen, S. Marder, *Chem. Mater.* **2011**, *23*, 4002–4015.
[10] B. Li, L. Zhou, H. Cheng, Q. Huang, J. Lan, L. Zhou, J. You, *Chem. Sci.* **2018**, *9*, 1213–1220.
[11] Y. Tao, Q. Wang, C. Yang, Q. Wang, Z. Zhang, T. Zou, J. Qin, D. Ma, *Angew. Chem. Int. Ed.* **2008**, *47*, 8104–8107.
[12] X. Wu, L. Wang, Y. Hua, C. Wang, A. S. Batsanov, M. R. Bryce, *Tetrahedron* **2014**, *70*, 2015–2019.
[13] Q. Li, L.-S. Cui, C. Zhong, Z.-Q. Jiang, L.-S. Liao, *Org. Lett.* **2014**, *16*, 1622–1625.
[14] S. Gong, Q. Fu, W. Zeng, C. Zhong, C. Yang, D. Ma, J. Qin, *Chem. Mater.* **2012**, *24*, 3120–3127.
[15] D. Zhang, X. Cao, Q. Wu, M. Zhang, N. Sun, X. Zhang, Y. Tao, *J. Mater. Chem. C* **2018**, *6*, 3675–3682.

[16] S. Chidirala, H. Ulla, A. Valaboju, M. R. Kiran, M. E. Mohanty, M. N. Satyanarayan, G. Umesh, K. Bhanuprakash, V. J. Rao, *J. Org. Chem.* **2016**, *81*, 603–614.
[17] J. Zhang, L. Zhou, H. A. Al-Attar, K. Shao, L. Wang, D. Zhu, Z. Su, M. R. Bryce, A. P. Monkman, *Adv. Funct. Mater.* **2013**, *23*, 4667–4677.
[18] Y. Zheng, A. S. Batsanov, V. Jankus, F. B. Dias, M. R. Bryce, A. P. Monkman, *J. Org. Chem.* **2011**, *76*, 8300–8310.
[19] W. Yu, G. Huang, Y. Zhang, H. Liu, L. Dong, X. Yu, Y. Li, J. Chang, *J. Org. Chem.* **2013**, *78*, 10337–10343.
[20] B. Akhlaghinia, S. Rezazadeh, *J. Braz. Chem. Soc.* **2012**, *23*, 2197–2203.
[21] R. Huisgen, J. Sauer, H. J. Sturm, J. H. Markgraf, *Chem. Ber.* **1960**, *93*, 2106–2124.
[22] S. Kun, G. Z. Nagy, M. Tóth, L. Czecze, A. N. Van Nhien, T. Docsa, P. Gergely, M.-D. Charavgi, P. V. Skourti, E. D. Chrysina, *Carbohydr. Res.* **2011**, *346*, 1427–1438.
[23] G. Méhes, K. Goushi, W. J. Potscavage, C. Adachi, *Org. Electron.* **2014**, *15*, 2027–2037.
[24] P. L. Santos, J. S. Ward, P. Data, A. S. Batsanov, M. R. Bryce, F. B. Dias, A. P. Monkman, *J. Mater. Chem. C* **2016**, *4*, 3815–3824.
[25] R. Ishimatsu, S. Matsunami, K. Shizu, C. Adachi, K. Nakano, T. Imato, *J. Phys. Chem. A* **2013**, *117*, 5607–5612.
[26] M. A. Baldo, C. Adachi, S. R. Forrest, *Phys. Rev. B* **2000**, *62*, 10967–10977.
[27] H. Yersin, A. P. Monkman, in *Highly Effic. OLEDs*, Wiley, Weinheim, **2018**, pp. 425–463.
[28] P. L. dos Santos, F. B. Dias, A. P. Monkman, *J. Phys. Chem. C* **2016**, *120*, 18259–18267.
[29] A. S. D. Sandanayaka, T. Matsushima, C. Adachi, *J. Phys. Chem. C* **2015**, *119*, 23845–23851.
[30] S. Höfle, M. Pfaff, H. Do, C. Bernhard, D. Gerthsen, U. Lemmer, A. Colsmann, *Org. Electron.* **2014**, *15*, 337–341.
[31] M. Regnat, K. P. Pernstich, B. Ruhstaller, *Org. Electron.* **2019**, *70*, 219–226.
[32] H. Nakanotani, K. Masui, J. Nishide, T. Shibata, C. Adachi, *Sci. Rep.* **2013**, *3*, DOI 10.1038/srep02127.

Manuscript received: April 18, 2019
Revised manuscript received: November 18, 2019